Climate Dynamics (2004) 23: 839–858
DOI 10.1007/s00382-004-0467-0

Filippo Giorgi · Xunqiang Bi · Jeremy Pal

Mean, interannual variability and trends in a regional climate change experiment over Europe. II: climate change scenarios (2071–2100)

Received: 19 December 2003 / Accepted: 3 June 2004 / Published online: 10 August 2004

Abstract We present an analysis of climate change over Europe as simulated by a regional climate model (RCM) nested within time-slice atmospheric general circulation model (AGCM) experiments. Changes in mean and interannual variability are discussed for the 30-year period of 2071–2100 with respect to the present day period of 1961–1990 under forcing from the A2 and B2 IPCC emission scenarios. In both scenarios, the European region undergoes substantial warming in all seasons, in the range of 1–5.5°C, with the warming being 1–2°C lower in the B2 than in the A2 scenario. The spatial patterns of warming are similar in the two scenarios, with a maximum over eastern Europe in winter and over western and southern Europe in summer. The precipitation changes in the two scenarios also show similar spatial patterns. In winter, precipitation increases over most of Europe (except for the southern Mediterranean regions) due to increased storm activity and higher atmospheric water vapor loadings. In summer, a decrease in precipitation is found over most of western and southern Europe in response to a blocking-like anticyclonic circulation over the northeastern Atlantic which deflects summer storms northward. The precipitation changes in the intermediate seasons (spring and fall) are less pronounced than in winter and summer. Overall, the intensity of daily precipitation events predominantly increases, often also in regions where the mean precipitation decreases. Conversely the number of wet days decreases (leading to longer dry periods) except in the winter over western and central Europe. Cloudiness, snow cover and soil water content show predominant decreases, in many cases also in regions where precipitation increases. Interannual variability of both temperature and precipitation increases substantially in the summer and shows only small changes in the other seasons. A number of statistically significant regional trends are found throughout the scenario simulations, especially for temperature and for the A2 scenario. The results from the forcing AGCM simulations and the nested RCM simulations are generally consistent with each other at the broad scale. However, significant differences in the simulated surface climate changes are found between the two models in the summer, when local physics processes are more important. In addition, substantial fine scale detail in the RCM-produced change signal is found in response to local topographical and coastline features.

F. Giorgi (✉) · X. Bi · J. Pal
Abdus Salam International Centre for Theoretical Physics, Trieste, Italy
E-mail: giorgi@ictp.trieste.it
Fax: +39-40-2240449

1 Introduction

This study presents an analysis of a new set of climate change simulations over the European region performed using a nested regional climate model (RCM) system. The companion paper by Giorgi et al. (2004) (hereafter referred to as GBP04) presented a validation of the present day (or "reference") simulation covering the period 1961–1990. Here, we turn our attention to the simulation of future climate conditions under different scenarios of changes in greenhouse gas (GHG) and aerosol concentrations.

Two 30-year scenario simulations are performed for the period 2071–2100, one for the A2 and the other for the B2 IPCC emission scenarios (IPCC 2000). The regional model used in the present work is the version of RegCM originally developed by Giorgi et al. (1993a, b) and later augmented as described by Giorgi and Mearns (1999) and Pal et al. (2000). The large scale fields needed to produce lateral boundary conditions for the RegCM simulations are obtained from corresponding time-slice experiments with a high resolution version of the Hadley Centre atmospheric general circulation model HadAM3H (Jones et al. 2001).

Following GBP04, we here investigate the average change in climatic variables, the change in interannual

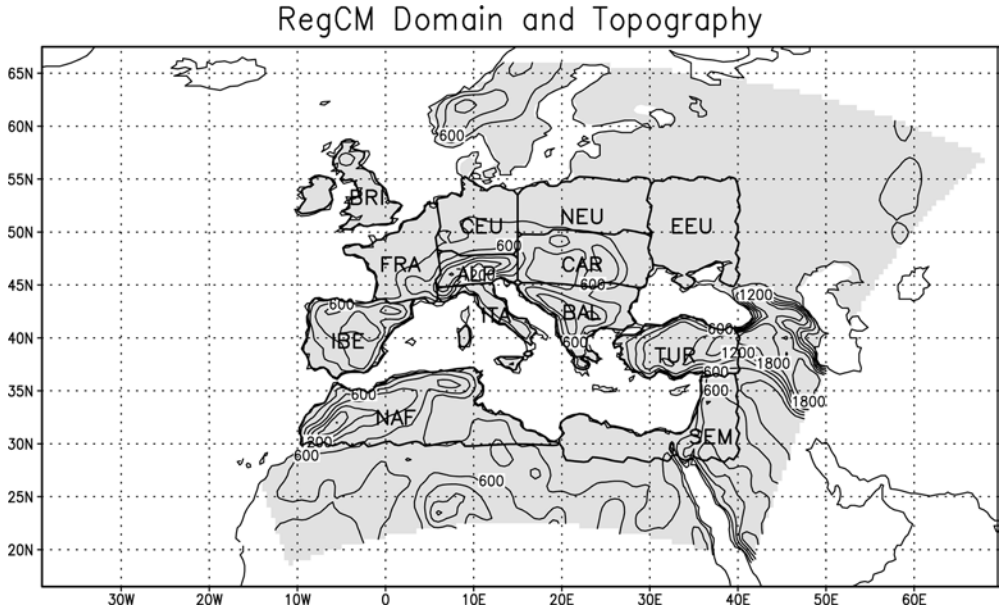

Fig. 1 RegCM domain and topography. Units are meter and the contour interval is 300 m. Also shown are 13 subregions used for more detailed analysis. *IBE* Iberian Peninsula, *ITA* Italian Peninsula, *BAL* Balkan Peninsula, *TUR* Turkey, *NAF* Northwest Africa, *SEM* Southeastern Mediterranean, *ALP* Alps, *FRA* France, *BRI* British Islands, *CEU* Central Europe, *CAR* Carpathian region, *NEU* Northeastern Europe, *EEU* Eastern Europe

variability and the trends in the scenario experiments. The latter two represent novel focus areas within the context of nested regional climate simulations, mostly because RCM experiments of sufficient length to obtain robust statistics have become available only recently. Examples of previous regional climate change simulations for the European region include Giorgi et al. (1992), Jones et al. (1997), Räisänen and Joelsson (2001), Räisänen et al. (2001 , 2004), Christensen and Christensen (2003), Schär et al. (2004), and Beniston (2004).

Our analysis is primarily centered on surface air temperature and precipitation, the two variables most used in impact assessment studies. However, we also examine the changes in circulation structure, cloudiness and surface hydrologic variables to better understand the surface climate change signals. Simple measures of daily precipitation statistics are investigated in order to elucidate how the average climatological changes are reflected in corresponding changes of statistics of weather events. The changes produced in the A2 and B2 experiments are intercompared to examine how regional climate change patterns depend on the forcing scenarios. The changes simulated by the nested RegCM and driving HadAM3H are then intercompared to evaluate the relative importance of the lateral boundary forcing and the internal model physics in determining the regional climate change signal.

The simulations analyzed in this study are part of the European project Prediction of Regional scenarios and Uncertainties for Defining EuropeaN Climate change risks and Effects (PRUDENCE, Christensen et al. 2002). In this project, a range of global and regional climate models are used within a common framework to produce climate change projections for the European region and to assess the related uncertainties via an intercomparison of the different model results.

2 Models and experiment design

The models used for the present study are already described in GBP04 and references therein. HadAM3H is described by Pope et al. (2000) and Jones et al. (2001). Its horizontal grid interval is 1.25° latitude by 1.875° longitude. The model includes a full sulfur cycle to calculate the concentration of sulfate aerosols from the emission of DMS and SO_2. Both direct and indirect aerosol radiative effects are represented.

The version of RegCM used for the regional model simulations is described in detail by Giorgi et al. (1993a, b), Giorgi and Mearns (1999) and Pal et al. (2000). The model grid interval is 50 km, and its domain and topography are shown in Fig. 1 a long with 13 subregions selected for more detailed analysis. These are the same regions used in the validation study of GBP04 and the portion of the domain encompassed by these regions represents our interest area. Many of the plots we present cover only this region in order to better illustrate the detail associated with local topography and coastlines.

The RegCM uses its standard vertical configuration of 14 sigma levels, model top at 80 hPa and five levels below about 1,500 m. The assimilation of lateral boundary conditions uses the modified relaxation technique described by Giorgi et al. (1993b). The RegCM also includes both direct and indirect sulfate aerosol effects as described by Giorgi et al. (2002, 2003a) and GBP04.

►

Fig. 2 Difference between A2 (2071–2100) and reference (1961–1990) SLP and 500 hPa geopotential height in the RegCM simulations: **a** SLP, DJF, **b** 500 hPa height, DJF, **c** SLP, JJA, **d** 500 hPa height, JJA. Units are hecta Pascal for the SLP and meter for the 500 hPa geopotential height

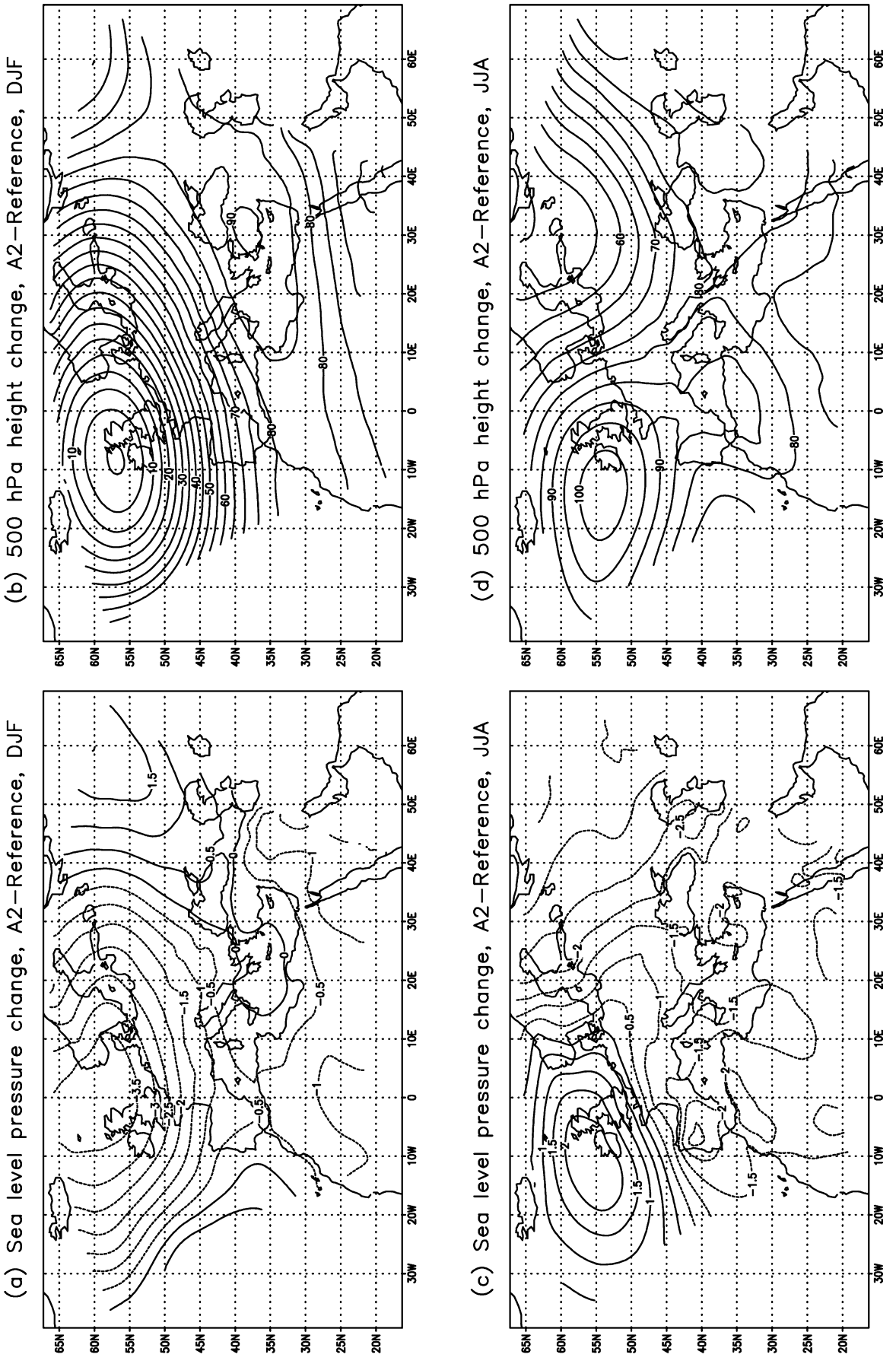
(a) Sea level pressure change, A2−Reference, DJF
(b) 500 hPa height change, A2−Reference, DJF
(c) Sea level pressure change, A2−Reference, JJA
(d) 500 hPa height change, A2−Reference, JJA

Simulations for both the A2 and B2 IPCC (2000) emission scenarios are performed for the 30-year period of 2071–2100. Within the full range of the IPCC emission scenarios, the A2 lies towards the upper end, with a CO_2 concentration of about 850 ppm by 2100, while the B2 scenario lies towards the lower end, with a CO_2 concentration of about 600 ppm by 2100. The two scenarios encompass about half of the IPCC emission scenario range.

The experiment design is as follows (Jones et al. 2001). The reference HadAM3H simulation used to drive the corresponding RegCM experiment utilizes observed sea surface temperature (SST), sea-ice distribution, concentrations of GHG (CO_2, CH_4, N_2O and CFCs) and emissions of DMS and SO_2 for the period 1961–1990 (see GBP04). For the scenario simulations, GHG concentrations and DMS and SO_2 emissions are specified from the corresponding emission scenarios (A2 or B2, see IPCC 2000 and Johns et al. 2001). For the SST and sea-ice distribution a spatially varying monthly perturbation is added to the reference values as calculated from corresponding transient experiments with the Hadley Centre coupled model HadCM3 (Johns et al. 2001; Jones et al. 2001). The perturbation is calculated for each month (January, February, March, etc.) and consists of an average monthly value (2071–2100−1961–1990) plus a linear trend for the 2071–2100 period calculated separately for each month. This implies that the SST interannual variability in the scenario simulations is similar to that in the reference simulation except for the underlying trend.

For the corresponding regional model simulations, the SST, sea-ice, GHG and sulfate concentrations used (or calculated) by HadAM3H are directly interpolated onto the RegCM grid and used by the model to calculate the resulting radiative forcing. SST and sea-ice are updated monthly, GHG concentrations every 10 years and sulfate concentrations every 6 h, with a linear interpolation between successive updates at each RegCM time step. Note that, both for the reference and the scenario simulations the HAdAM3H fields needed to produce the RegCM lateral meteorological boundary conditions were provided on a coarser grid than the original HadAM3H one, and more specifically on a 2.5° latitude by 3.75° longitude grid. In addition, the surface vegetation and landuse distribution in the RegCM is the same in the scenario and reference simulations and is obtained from a global dataset produced by the United States Geological Survey from satellite observations (e.g. Loveland et al. 1991).

For brevity, we do not show here the SST perturbation field and only give a brief description of it. In the winter season, for the A2 scenario the SST perturbation varies in the range of 0.5–2.5°C over the northeastern Atlantic and 2–3°C over the Mediterranean, North Sea and Black Sea. In summer, the SST perturbation for the A2 scenario is in the range of 0.5–2.5°C over the northeastern Atlantic, 2.5–4.5°C over the Mediterranean and North Sea, and 4.5–5.5°C over the Black Sea. A special mention should go to the Baltic Sea, for which the SST perturbation calculated by the HadCM3 model is in the range of 2.5–3.5°C in winter and 5–7°C in summer. As we will see, this large summer Baltic SST increase has a substantial impact on the simulated climate change signal over the downwind regions. In the B2 scenario the SST perturbation is generally 1–2°C smaller than in the A2 scenario throughout the domain.

Finally, unless otherwise specified, we refer here to the term "change" as the difference between the selected climate statistics in the scenario (2071–2100) and reference (1961–1990) simulations.

Fig. 3 Difference between scenario (2071–2100) and reference (1961–1990) average surface air temperature over the interior domain in the RegCM simulations: **a** DJF, A2 scenario, **b** DJF, B2 scenario, **c** JJA, A2 scenario, **d** JJA, B2 scenario. Units are Celsius and the contour interval is 0.5°C. All changes are statistically significant at the 95% confidence level

3 Results

3.1 Seasonal mean changes

We begin our analysis with a discussion of the changes in large scale circulation patterns over our full domain as described by sea level pressure (SLP) and 500 hPa geopotential height fields. Figure 2 shows the change in average SLP and 500 hPa height between the A2 and reference simulations. Results are shown for December–February (DJF) and June–August (JJA), the two seasons for which the largest changes are found. Circulation changes in the HadAM3H fields are very similar to those in the RegCM simulation due to the large scale forcing by the lateral boundary fields, and are thus not shown. Also note that the changes in 500 hPa height in Fig. 2b, d are all positive. This is because of the lower tropospheric warming in the scenario simulations, which implies a thicker lower atmosphere. However, what determines the atmospheric circulations are the horizontal gradients in 500 hPa height, and thus the relative minima and maxima in Fig. 2b, d.

In DJF, we find an area of reduced SLP and increased cyclonic circulation aloft centered over the North Sea/British Isles region and extending from the northeastern Atlantic to central and northern Europe. This is related to a corresponding southeastward oriented gradient in tropospheric warming pattern, and it is an indication of increased storm activity over this region. In JJA, we find an entirely different pattern of circulation change. In this case an increase of SLP dominates over the northeastern Atlantic off the western coasts of the British Isles with reduced SLP over central and eastern Europe (Fig. 2c). The associated change in circulation aloft shows a ridge over western Europe and a trough over northeastern Europe (Fig. 2d). This blocking-like change pattern causes a northward shift of the Atlantic storm track as it enters the European sector

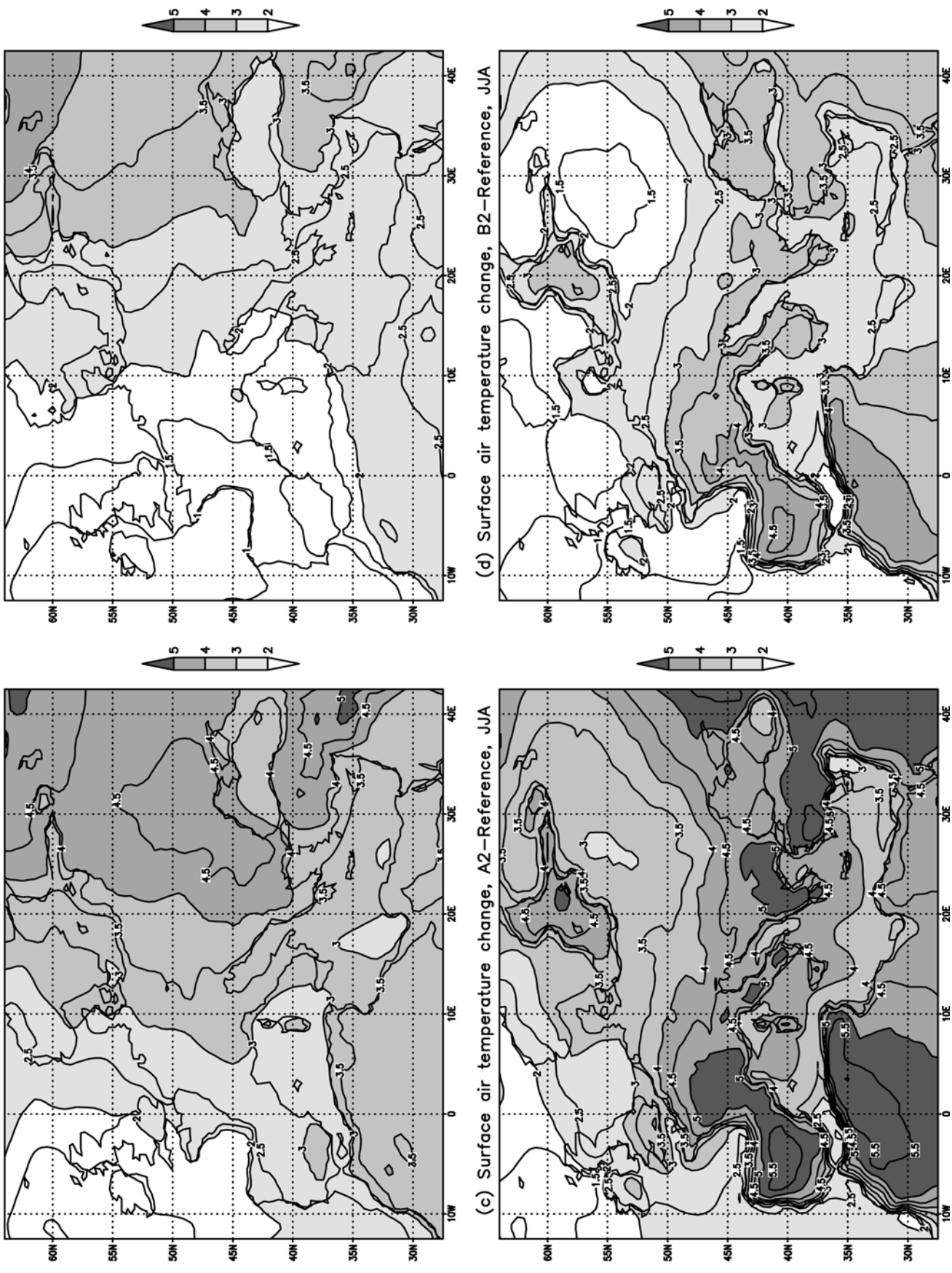
(a) Surface air temperature change, A2−Reference, DJF
(b) Surface air temperature change, B2−Reference, DJF
(c) Surface air temperature change, A2−Reference, JJA
(d) Surface air temperature change, B2−Reference, JJA
5 4 3 2
60N 55N 50N 45N 40N 35N 30N
10W 0 10E 20E 30E 40E

followed by a southward shift east of the Baltic Sea region. Circulation changes similar to those shown in Fig. 2 were found in the B2 scenario (not shown).

The effects of these circulation changes on the surface climate of our interest region are illustrated in Figs. 3 and 4, which show the DJF and JJA changes in surface air temperature and precipitation for the A2 and B2 RegCM simulations. Following the global warming due to the increased GHG concentration, in both scenarios and seasons a substantial warming occurs throughout the European region. The warming patterns show similar spatial features in the two scenarios, with the warming being about 1–2°C lower in the B2 than the A2 case.

In DJF, the warming is in the range of about 2–5°C in the A2 run and 1–4°C in the B2 run, and it increases from the western coastal regions to the eastern continental interiors (Fig. 3a, b). This gradient is at least partially tied to the increased advection of air from the northeastern Atlantic, which is characterized by a lower warming than found in the continental interior (see Fig. 2). In JJA, the warming is more pronounced than in DJF (Fig. 3c, d), about 3–5.5°C in the A2 case and 1.5–4.5°C in the B2 case, and shows a different spatial pattern. In fact, the Mediterranean and western European regions exhibit a maximum JJA warming, while the north-eastern European regions show an area of minimum warming. This feature of an amplified warming during the summer over southern Europe and the Mediterranean appears to be common in a number of climate change simulations for different scenarios (Giorgi et al. 2001; Räisänen et al. 2004) Note that the temperature changes in all seasons and for both the A2 and B2 scenarios are statistically significant at the 95% confidence level.

The precipitation change patterns show similar spatial structure in the two scenario simulations (Fig. 4), although winter precipitation decreases over the Mediterranean region less in the B2 than in the A2 scenario. Figure 4a, b shows a widespread and statistically significant increase in DJF precipitation over most of Europe north of about 42°N. This is due to at least two factors. The first is the increase in winter storm activity over the central-northern European regions (see Fig. 2a, b) and the second is an increase in water-holding capacity of the warmer atmosphere in the B2 and A2 scenarios. Although not shown for brevity, we found that, compared to the reference simulation, in DJF the vertically integrated atmospheric water vapor content increased over central and northern Europe by 25–40% in the A2 scenario and by 10–30% in the B2 scenario.

The DJF precipitation change exhibits a distinct north–south gradient, with the change reversing sign along a line that cuts across the Iberian, Italian and Balkan peninsulas. South of this line, from the southern Mediterranean to the northern Africa regions, the winter precipitation amounts decrease in the scenario simulations, with this decrease being statistically significant over extended areas in the A2 case and smaller areas in the B2 one. This decrease in DJF precipitation over southern Europe is mostly due to regionally increased anticyclonic circulation (see Fig. 2a, b), since the atmospheric moisture amounts are greater in both the A2 and B2 scenarios than in the reference simulation throughout the model domain (not shown).

In JJA, the blocking-type summer anticyclonic structure shown in Fig. 2c, d deflects the Atlantic storm track northward and causes a widespread decrease of precipitation over most of western Europe and the Mediterranean Basin (Fig. 4c, d), despite an increase in atmospheric moisture of 10–20% in both scenarios (not shown). The precipitation decrease is statistically significant at the 95% confidence level over most of the western European continental areas. A decrease in summer precipitation over the southern European regions has been also observed in a number of previous global (Giorgi et al. 2001) and regional climate simulations (Giorgi et al. 1992; Jones et al. 1997; Räisänen and Joelsson 2001; Räisänen et al. 2001, 2004; Christensen and Christensen 2003).

Conversely, in JJA the regions of western Russia downwind of the Baltic Sea show an increase in precipitation, although this is statistically significant only over relatively small land regions. Similarly to the DJF case, also in JJA the area of increased precipitation is more extended in the B2 than in the A2 run. The increase in precipitation over western Russia is attributable to two factors. The first is the southward shift of the jet simulated over this region (see Fig. 2d), which would tend to increase the number of storms crossing there. The second factor is related to the changes in Baltic SST simulated by HadCM3 and subsequently transmitted to HadAM3H and the RegCM. As mentioned, the Baltic SST shows a summer increase of several degrees, which results in enhanced evaporation from the sea and increased precipitation over the downwind regions of northeastern Europe.

The patterns of change in circulation, surface air temperature and precipitation in the intermediate seasons of March–May (MAM) and September–November (SON) are not shown for brevity (regional averages are reported in Figs. 8, 9, 10 and 11). In MAM, the changes are somewhat similar to those found in DJF, namely an increase in storminess and precipitation over central and northeastern Europe and a corresponding decrease over southern Europe and the Mediterranean Basin. Conversely, the circulation and precipitation changes in SON are more similar to those found in JJA, with widespread decrease of precipitation throughout Europe except for the Baltic Sea region.

An important aspect of the changes in Figs. 3 and 4 is the fine scale structure of the change signal associated with coastlines and topography. For temperature, this is especially evident in JJA over the Mediterranean area (Fig. 3c, d), where the land–ocean contrast in warming associated with the Iberian, Italian, Balkan and Turkish Peninsulas and large Islands can exceed 1°C. The topographical forcing of these Peninsulas on the pre-

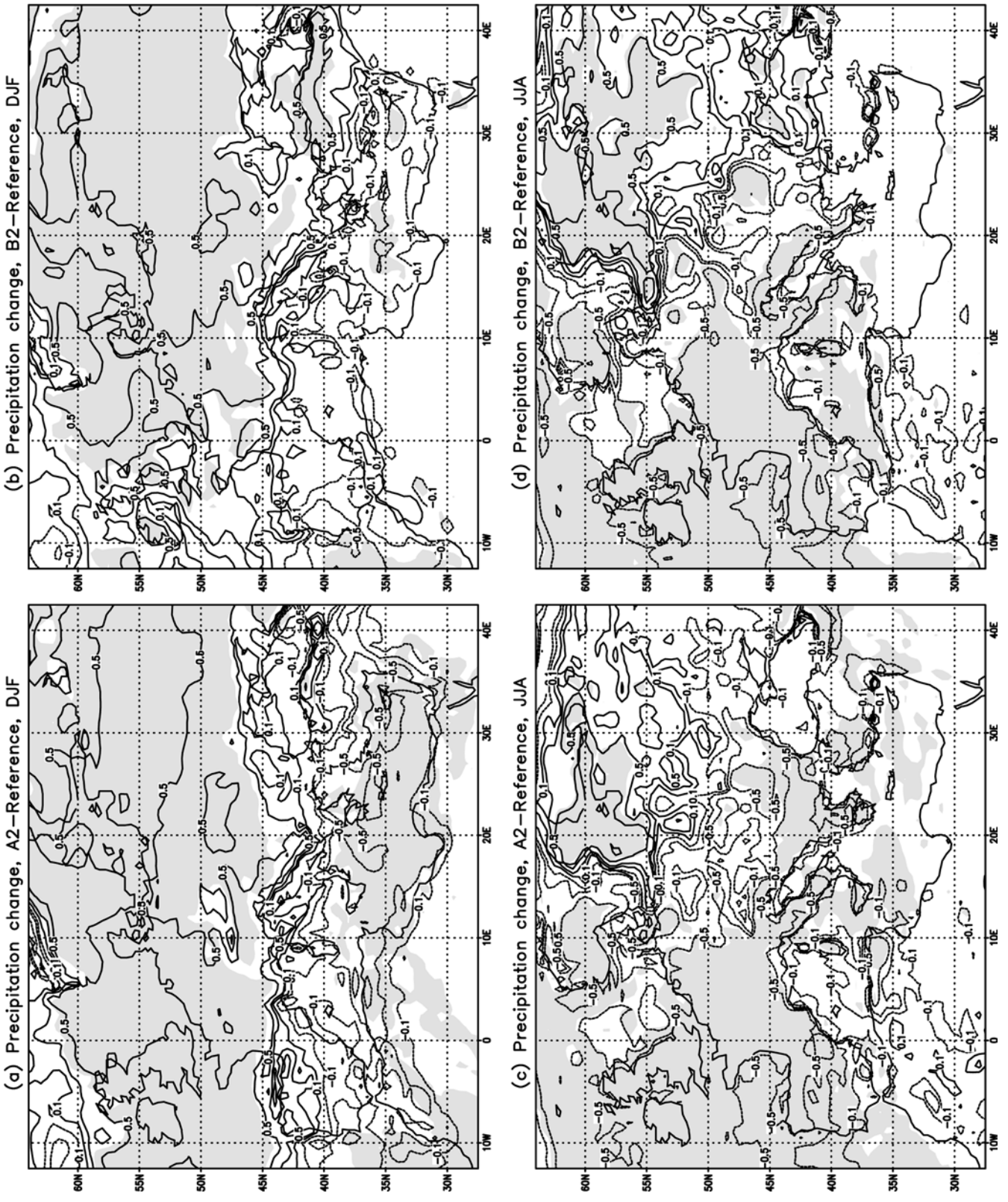

Fig. 4 Difference between scenario (2071–2100) and reference (1961–1990) mean precipitation over the interior domain in the RegCM simulations: **a** DJF, A2 scenario, **b** DJF, B2 scenario, **c** JJA, A2 scenario, **d** JJA, B2 scenario. Units are millimeter per day and the contour lines are at −0.5, −0.25, −0.1, 0, 0.1, 0.25 and 0.5 mm/day. *Shading* indicates areas where the change is statistically significant at the 95% confidence level

cipitation change signal is also evident in both seasons, as it is over the Scandinavian and Alpine regions. In addition to topography, land–sea contrasts in latent heat and sensible heat flux affect the change signals during the summer.

These considerations point to the necessity of fine scale climate information over the European region. For brevity we do not show here the patterns of temperature and precipitation change simulated by the HadAM3H forcing fields (regionally averaged HadAM3H changes are reported in Figs. 8, 9, 10 and 11), but their broad scale spatial structure is similar to that of the RegCM, since the broad scale climatic features in the nested model are essentially driven by the forcing lateral fields. On the other hand, the regional spatial detail is necessarily coarser in HadAM3H due to its coarser resolution.

The regional changes in temperature and precipitation are affected by changes in cloudiness and soil water content, which in turn influence the surface energy and water budgets. Changes in cloudiness (as measured by the total fractional cloud cover) and soil water content of the root zone for the A2 scenario are shown in Figs. 5 and 6, respectively (similar change patterns were found in the B2 scenarios, not shown). The distribution of DJF cloudiness change (Fig. 5a) mostly follows the distribution of precipitation change (Fig. 4a), with increase over central and northern Europe and decrease over the Mediterranean and northern Africa. The change in cloud water content (not shown), which affects the optical cloud water path, also showed patterns generally similar to those of the precipitation changes. The net effect of cloudiness changes on the DJF surface temperature is difficult to evaluate, since greater cloud amounts reduce the incoming solar radiation at the surface, but also increase the downward infrared radiation. In winter these two competing effects are on average of similar magnitude, and indeed a cloud signal on the DJF temperature change is not evident.

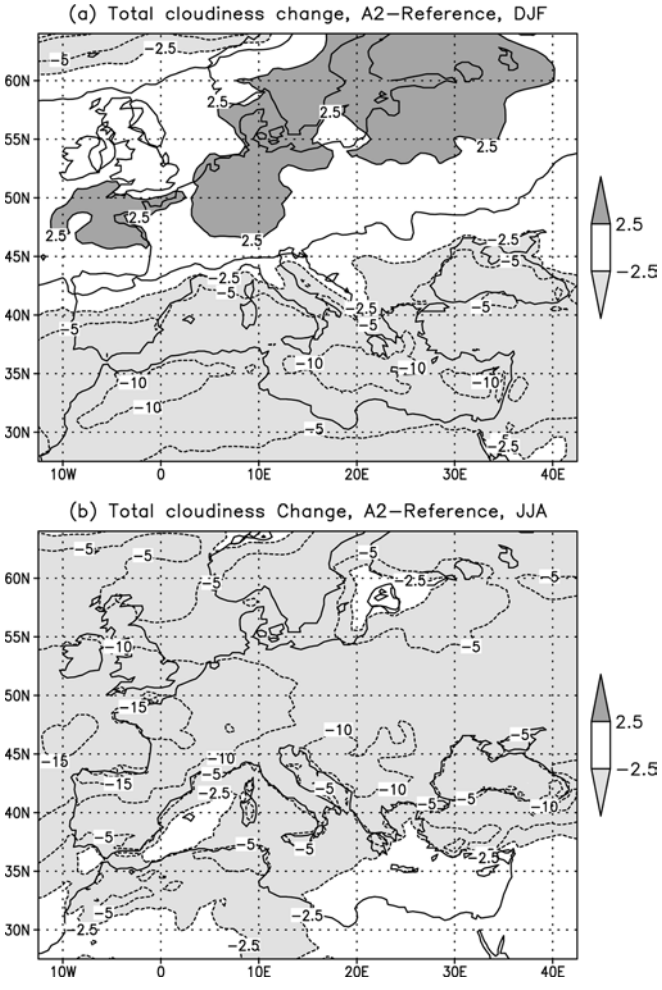

Fig. 5 Difference between A2 (2071–2100) and reference (1961–1990) mean cloudiness over the interior domain in the RegCM simulations: **a** DJF, **b** JJA. Units are fractional cloud cover in percentage and contour lines are at −15, −10, −5, −2.5, 0, 2.5, 5, 10, 15%. The *thicker line* indicates the 0 value

Figure 6a shows that in DJF the root zone water content decreases over most of western Europe despite an increase of precipitation there. This is due to two contributions: First, the soil-water loss due to increased evapotranspiration rates at the higher A2 surface temperatures is not counterbalanced by the soil-water input from increased precipitation; second, the deep soil-water which has been severely depleted in the scenario runs during the preceding summer fails to recover to reference run values during the winter. Exceptions to this pattern are found over the Alps, the mountains of northern Turkey and central Asia and regions of western Russia, where the winter soil moisture actually increases. This can be attributed to the increased soil-water input from winter snowmelt under the A2 warming conditions (see below), which prevails over the loss due to increased evapotranspiration.

In JJA, both cloudiness and root zone soil-water content show a decrease throughout most of Europe (Figs. 5b and 6b). The corresponding reduction in evapotranspiration and enhancement in surface solar flux tend to enhance the summer warming and drying over the region. Downwind of the Baltic Sea, summer soil-water and cloudiness show a minimum decrease (Figs. 5b and 6b) because of enhanced precipitation there. This in turn leads to the minimum JJA warming found in Fig. 3c. This minimum is further amplified by the enhanced northwesterly advection of relatively cool arctic air over central-eastern Europe (see Fig. 2d). This finding, however, should be taken cautiously because an important contribution to it is from the increase in Baltic SST simulated by the coarse resolution HadCM3, and more detailed simulations are required to assess this result.

It is interesting to note from the comparison of Figs. 4 and 5, that changes in cloudiness and precipitation, although generally similar in spatial pattern, show an important difference. Specifically, the areas of decreased cloudiness are generally more extended than the areas of decreased precipitation, i.e. some regions where

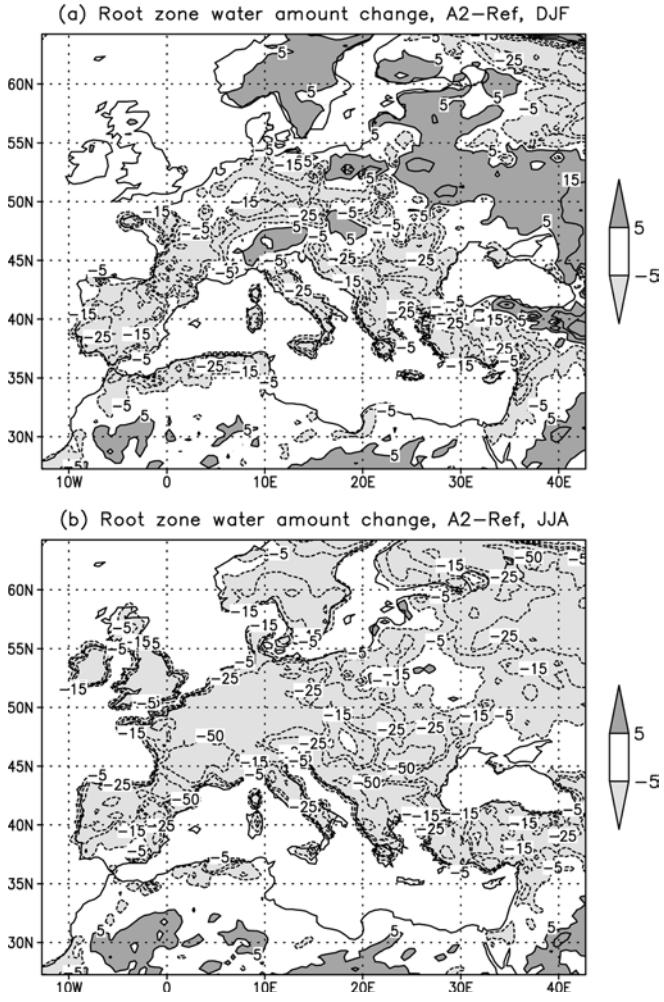

Fig. 6 Difference between A2 (2071–2100) and reference (1961–1990) soil water content of the root zone over the interior domain in the RegCM simulations: **a** DJF, **b** JJA. Units are millimeter of water and contour lines are at −50, −25, −15, −5, 0, 5, 15, 25, 50 mm

precipitation increases show a decrease in cloudiness. This effect was indeed evident also in MAM and SON, where cloudiness decreased over most of the domain even when precipitation increased. Conversely, the changes in cloud water content more closely followed the precipitation changes. Since, the cloud fractional cover mostly depends on the grid point relative humidity while precipitation depends on the cloud liquid-water content (Pal et al. 2000), this finding suggests that the precipitation efficiency (defined as the ratio of precipitation over the total cloud water column) in the scenario simulations is enhanced, since a more efficient removal of water from the atmosphere via precipitation implies that less water is available to moisten the grid point and generate clouds.

Similarly, the areas of decreased root zone soil-water are generally more extended than the areas of decreased precipitation, both in DJF and JJA (compare Figs. 4 and 6). This implies that the water loss due to increased evapotranspiration at the warmer scenario temperatures tends to dominate over the enhanced water input due to increased precipitation. This leads to a general drying of European soils in the scenario simulations.

An additional factor that contributes to modulate the surface warming is the change in surface snow cover and the resulting change in surface albedo. Figure 7 shows the average DJF snow amount in the reference run and the difference between DJF snow in the A2 and reference simulations. Clearly distinguishable in the reference run, even at the relatively smooth model topography, are the snowpacks over the Alps, the Carpathian mountains of central Europe, the coastal chains of the Scandinavian Peninsula and the mountain chains of Turkey and central Asia. The average snow amounts also increase towards northeast Russia.

In the A2 simulation winter snow amounts are substantially depleted throughout continental Europe. A strong snow depletion is found in particular over all mountain chains and over eastern Europe. Giorgi et al. (1997) first pointed out how changes in snow cover can modulate the surface temperature change signal through the snow albedo feedback mechanism. If the GHG-induced warming depletes the snow cover, the surface albedo decreases; this leads to more solar radiation reaching the surface, which in turn enhances the surface warming, accelerates the snow depletion and sustains a positive feedback mechanism. In the simulations of Giorgi et al. (1997), as well as in those of Leung and Ghan (1999), this mechanism induced an elevation modulation of the temperature change signal. Such a modulation, although not a dominant signal, is found also in our run over the Alps and the mountains of Turkey and central Asia. In addition, comparison of Figs. 3 and 7 indicates that the snow depletion might also provide an important contribution to the amplification of the DJF warming signal found over the areas north of the Black Sea, where the snowpack is heavily depleted.

The surface air temperature changes for both scenarios and for all seasons averaged over the 13 regions of Fig. 1 are summarized in Fig. 8. The regionally averaged warming in the A2 scenario varies in the range of 2–5°C over most regions and seasons, with minimum warming occurring consistently over the British Isles and the Iberian Peninsula due to the ameliorating effect of the northeastern Atlantic ocean waters. The magnitude of regional warming in the B2 scenario is about 1–2°C smaller than in the A2 scenario across seasons. The most pronounced inter-regional variability of warming is found in the extreme seasons, DJF and JJA, while the intermediate seasons (MAM and SON) show a more uniform warming across regions.

Comparison of the regional warming magnitudes in the HadAM3H and RegCM simulations shows that these are generally close to each other in all seasons except JJA, when the RegCM shows a lower warming than HadAM3H by up to 1–2°C. This is an indication that in DJF, MAM and SON the regionally averaged warming is strongly forced by the HadAM3H lateral boundary fields. Conversely, in JJA local physical pro-

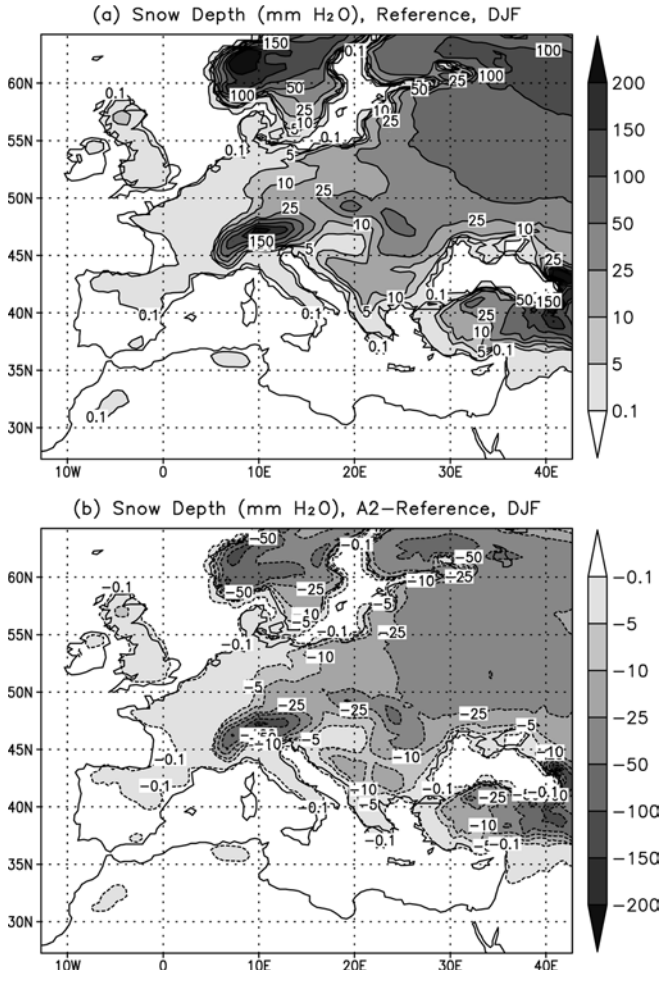

Fig. 7 Average DJF snow depth over the interior domain in the reference simulation **a** and difference between A2 (2071–2100) and reference (1961–1990) DJF snow depth **b** over the interior domain in the RegCM simulations. Units are millimeter of water equivalent and contour lines are at ±0.5, 5, 10, 25, 50, 100, 150, 200 mm

cesses related to land–atmosphere exchanges and convective activity become increasingly important and the internal physics and resolution of the two models play a more dominant role. In fact, Fig. 8 shows that the difference between RegCM and HadAM3H summer warming values is comparable in magnitude to the difference between the warming in the A2 vs. the B2 scenario. Note that in their simulation Räisänen et al. (2004) found warming values closer to those of HadAM3H over southern Europe. This may be due at least partially to the closer proximity of the southern European region to the southern lateral boundary in their domain, which would increase the lateral boundary forcing over this region.

As discussed in more detail by GBP04, the HadAM3H and RegCM models differ in their representation of surface processes, cumulus convection and planetary boundary layer physics, which in turn affect the vertical heat and moisture transfer. In this regard, the RegCM is characterized by a more efficient vertical transport than HadAM3H (see GBP04) and thus a tighter coupling between the surface and the troposphere. Since in general the effect of the GHG warming is maximum at the surface and tends to decrease in the upper troposphere, this enhanced surface–troposphere coupling would tend to reduce the surface warming in the regional model compared to HadAM3H.

Another important factor that affects the simulated warming is the change in precipitation. Figure 9 shows that in JJA, HadAM3H tends to consistently produce a greater decrease in precipitation than the RegCM. The resulting drier soil conditions in the future climate simulation would further contribute to amplify the warming in HadAM3H compared to the RegCM.

A feature to notice in the regional warmings of Fig. 8 is the similarity of the inter-regional variations of warming between the A2 and B2 scenarios, also reflected in the similarity of the A2 and B2 change patterns of Fig. 3. Figure 10a shows the ratio of A2 over B2 seasonal warming over the different European regions for the RegCM simulations (similar results were found in the HadAM3H experiments). It is evident that this ratio does not vary greatly across regions, being mostly in the range of 1.3–1.7. Giorgi and Mearns (2002) found that, when averaging results from nine different global model simulations, the ratio of A2 over B2 warming for 22 regions of sub-continental size across the globe was in the range of 1.3–1.5, a range approximately centered around the A2/B2 ratio of the ensemble average global temperature changes of 1.38. Given the smaller size of our regions compared to those of Giorgi and Mearns (2002) (our entire European domain is enclosed in two of the Giorgi and Mearns regions) and the fact that we are calculating the A2/B2 ratio from simulations with one model rather than an ensemble of different model simulations, our results appear consistent with those of Giorgi and Mearns (2002). They provide some support to the approach of scaling regional temperature responses to different forcing scenarios by a model's global temperature response (e.g. Mitchell et al. 1999).

The regionally-averaged precipitation changes for all scenarios and seasons are presented in Fig. 9. The precipitation change signal exhibits several different features from the temperature change signal. First, the sign of the change varies across seasons and regions because, as seen in the previous discussion, the precipitation change is mostly determined by changes in regional circulation patterns and atmospheric water holding capacity. The precipitation changes are predominantly positive in DJF, except for the southern Mediterranean and northern Africa regions, and negative in JJA. Mostly negative changes are also found in SON, while a more mixed change signal occurs in MAM. The extreme seasons (DJF and JJA) show the most pronounced changes, up to 15–30% over the western and central European regions in DJF, and up to 30–45% over the Mediterranean and western European regions in JJA. As noted in Fig. 4, these changes are mostly statistically significant at the 95%

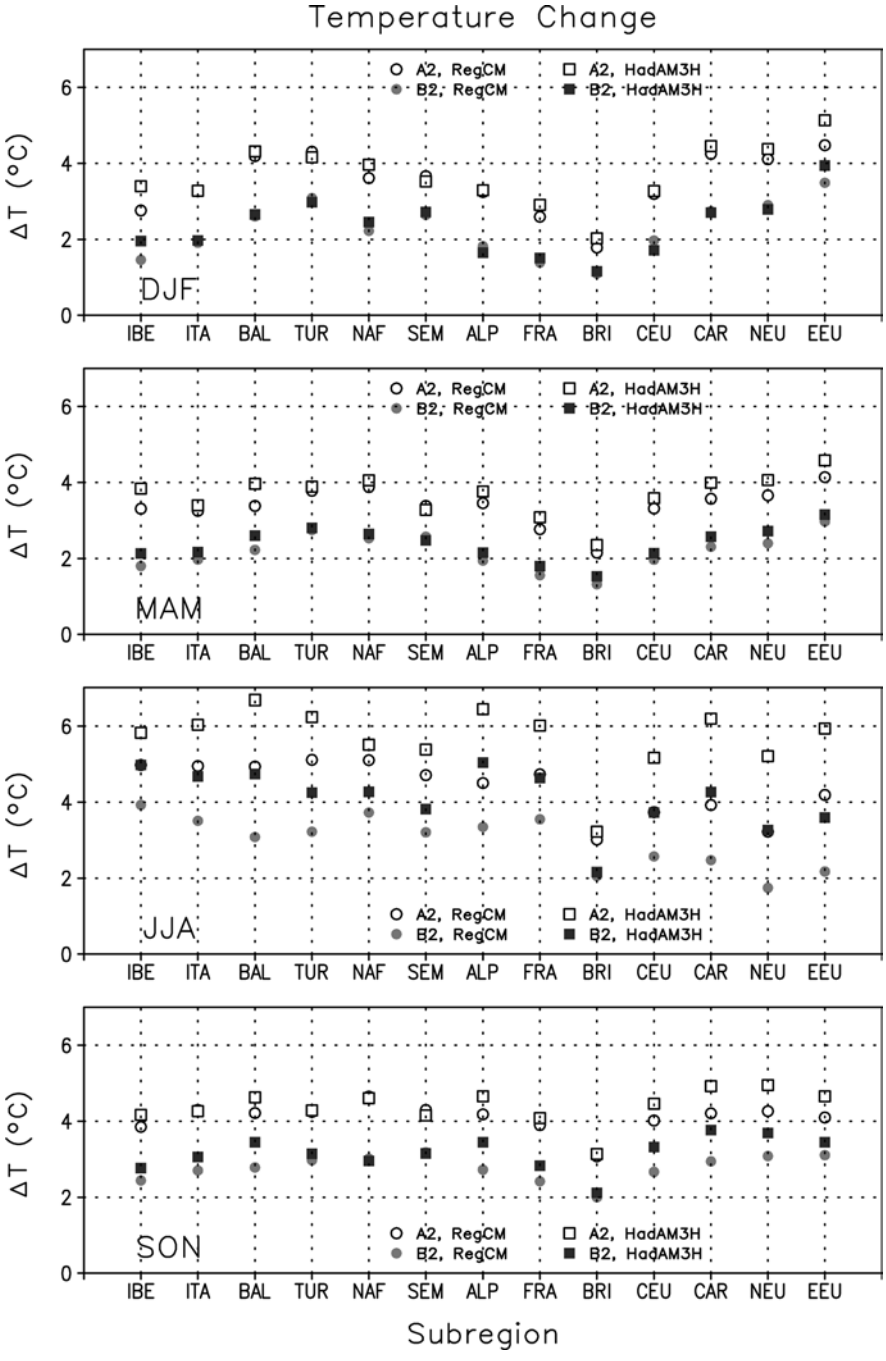

Fig. 8 Surface air temperature change averaged over the 13 regions of Fig. 1 for the A2 and B2 scenarios and the HadAM3H and RegCM simulations: **a** DJF, **b** MAM, **c** JJA, **d** SON. Units are in °celsius

confidence level. Conversely, the precipitation changes in the intermediate seasons (MAM and SON) are within $\pm 15\%$ except for a few cases, and are mostly not statistically significant.

Similar to the case of the temperature change, also for precipitation a general similarity in the regionally averaged changes is found between the RegCM and HadAM3H simulations except in JJA, where the HadAM3H simulates greater drying than the RegCM over most regions. Some noticeable differences between RegCM and HadAM3H also occur in MAM and SON over a number of regions. These are evidently due to the effects of the local topographical and coastline forcings as well as the model descriptions of physical processes.

Figure 10b shows the ratio of A2 over B2 regional precipitation changes for the cases in which the B2 change is greater than 5% (to avoid instances of small changes spuriously amplifying this ratio). The first feature to notice is the much wider range of A2/B2 change ratios for precipitation compared to temperature. This ratio varies from less than 1 to greater than 2. Secondly, the ratio is positive in almost all cases, implying the same sign of change (be it positive or negative) in the two scenarios. This is consistent with the precipitation

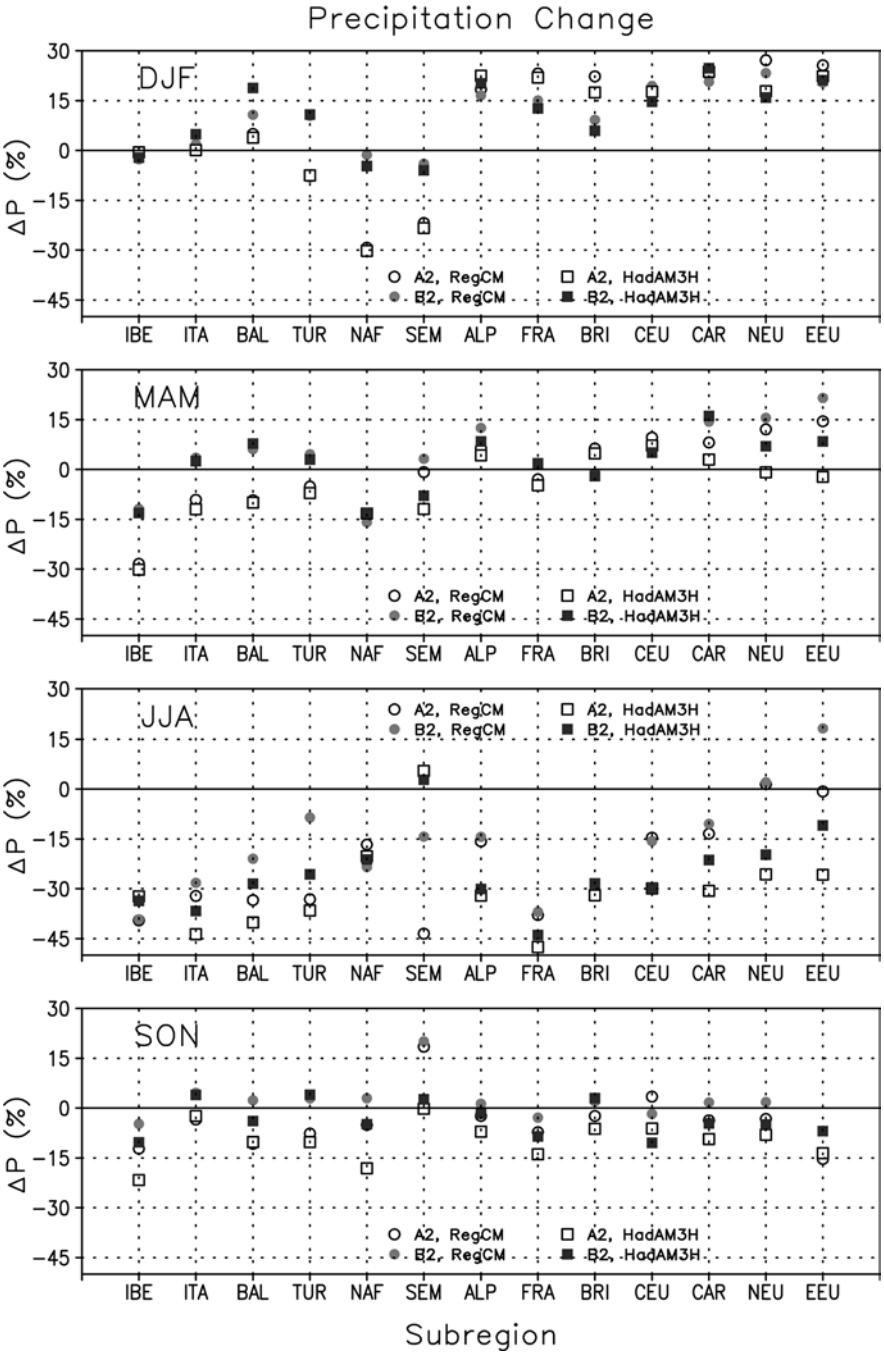

Fig. 9 Precipitation change averaged over the 13 regions of Fig. 1 for the A2 and B2 scenarios and the HadAM3H and RegCM simulations: **a** DJF, **b** MAM, **c** JJA, **d** SON. Units are percent of reference (1961–1990) values

change patterns shown in Fig. 4. Thirdly, in the majority of cases the A2/B2 precipitation change ratio is close to 1, that is the changes in the A2 and B2 scenarios are of similar magnitude.

3.2 Changes in daily precipitation characteristics

We plan to comprehensively analyze the statistics of daily precipitation and extreme events in a separate context. However, in order to gain a more complete picture of the nature of the precipitation changes, we present here the changes in some basic daily precipitation statistics. Figure 11 shows the changes in mean precipitation, average precipitation intensity and number of wet days for our 13 sub-regions in the A2 RegCM experiment. A wet day is defined by a precipitation amount exceeding 1 mm and the average intensity of precipitation is calculated by averaging the precipitation intensity only for the wet days. The regional calculations are performed by first computing the mean, average intensity and wet day number at each grid point and then averaging the grid point values over each region. Only land points were included in the calculations.

Figure 11 provides some important indications on the modes of change of precipitation statistics in the

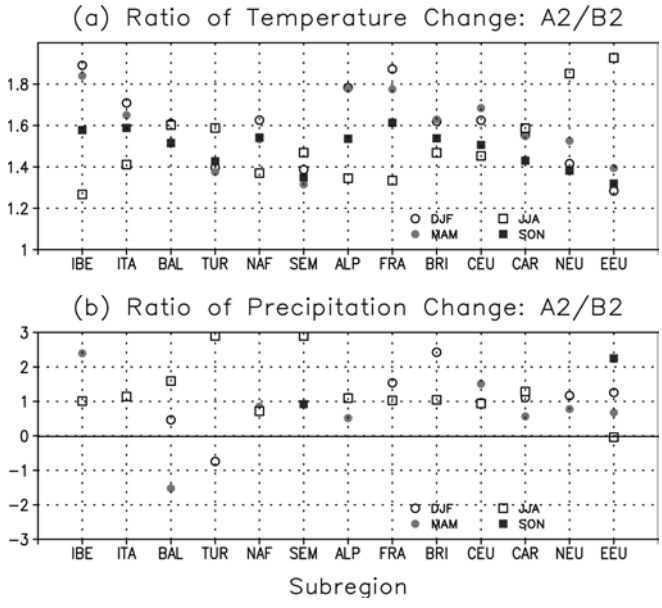

Fig. 10 Ratio between A2 and B2 changes in **a** surface air temperature and **b** precipitation for the 13 regions of Fig. 1 in the RegCM simulations. In panel **b** only regions are shown for which the B2 precipitation change is at least 5% in magnitude

RegCM. The most evident is that the average intensity of precipitation events tends to increase in the scenario simulation quite consistently across regions and seasons (with a small number of exceptions). In DJF, the increase in mean precipitation over the western and central European regions is due to an increase in both the precipitation intensity and the number of precipitation events, i.e. more frequent (or longer) and more intense storms occur over these regions in winter. This result is consistent with the increase in cyclonic activity suggested by Fig. 2 (more frequent events) and the increase in water vapor amounts in the scenario simulations (more intense events, see also Sect. 3.1). As a result, the percentage increase in mean precipitation is greater than the percentage increase in precipitation intensity. This behavior is unique across the seasons.

In the intermediate seasons of MAM and SON we mostly find small changes in mean precipitation. These are however consistently associated with substantial increases in precipitation intensity and corresponding decreases in wet day frequencies. Therefore in these seasons, although the mean precipitation is not substantially affected by the GHG forcing, the mode of precipitation is modified, with less frequent but more intense events occurring.

Finally, as also seen in Fig. 9, in most JJA cases and a number of cases for the other seasons (especially over the Mediterranean regions) the mean precipitation shows decreases, in many instances of large magnitude. Figure 11 indicates that this is essentially due to a corresponding decrease in the number of precipitation events that, on average, have a similar and in some areas higher intensity compared to the reference simulation. Similar conclusions were found for the B2 scenario (not shown for brevity).

Changes in precipitation characteristics can be also associated with changes in the mode of precipitation. We found that, in DJF, MAM and SON the fraction of total precipitation due to convection increased in the scenario simulations compared to the reference run (not shown). Greater convective activity along with higher water vapor loadings may thus be the causes of the greater intensity of events in these seasons. The convective precipitation fraction in JJA predominantly decreased in the scenario runs over the Mediterranean regions (not shown). This is an indication of lower buoyant energy production in the scenario simulations, probably a result of increased subsidence. In terms of precipitation intensity, this effect is however counterbalanced by the increased atmospheric water vapor amounts found in this season (see Sect.3.1).

In summary, Fig. 11 gives a predominant picture of precipitation events characterized by stronger intensity and occurring less frequently in the scenario simulations compared to the reference conditions (with the exception of DJF). This implies not only shifts in the intensity distribution of precipitation events, but also changes in the shape of this distribution. This picture of more intense events is conceptually consistent with the intensification of the hydrologic and energy cycles expected under warming conditions. It is also consistent with some analyses of changes in extreme events over the European region recently reported (Christensen and Christensen 2003; Huntingford et al. 2003; Räisänen et al. 2004).

3.3 Changes in interannual variability

As a measure of temperature interannual variability GBP04 used the interannual standard deviation of seasonal temperature calculated over the 30 years of the simulations. The coefficient of variation was instead adopted as a measure of precipitation variability in order to remove the dependency of the standard deviation on the mean precipitation. The same measures of variability are adopted in this work. However, the standard deviation and coefficient of variation are here calculated after first removing the linear trends of the seasonal values throughout the 30 year simulation periods. This is done in order to filter out the effect of the trends on the calculated variability measures, which is important primarily in the scenario simulations (see Sect.3.4).

Figures 12 and 13 show the changes in temperature and precipitation interannual variability, respectively, for the regions of Fig. 1 and for both the A2 and B2 scenario simulations. Results from the RegCM and HadAM3H experiments are compared, and changes are highlighted which are statistically significant at the 90% confidence level according to a standard *F*-test (von Storch and Zwiers 1999). For temperature, the variability changes are generally moderate in both models

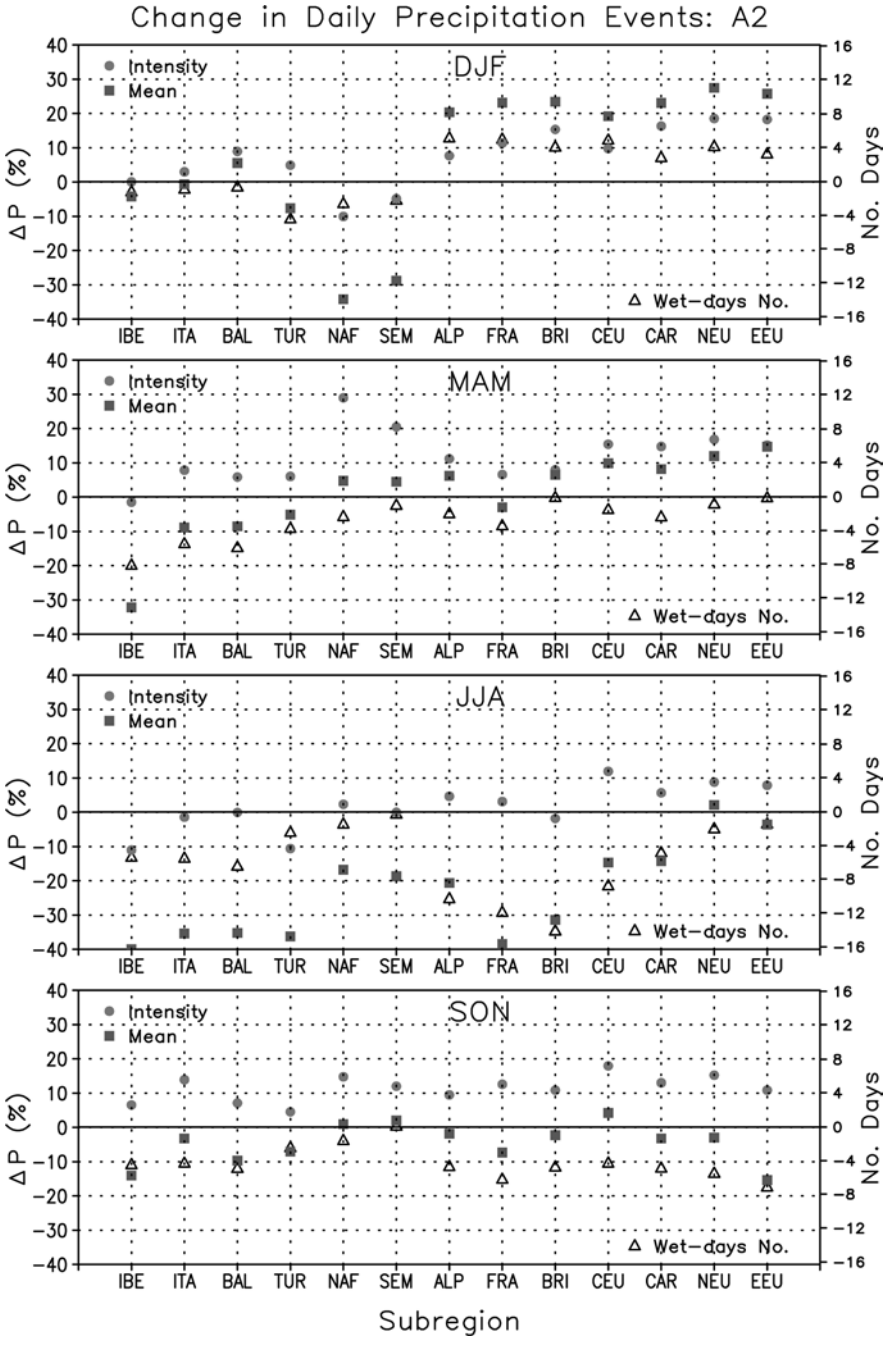

Fig. 11 Change in mean precipitation, average precipitation intensity and number of wet days for the A2 scenario RegCM simulation averaged over the 13 regions of Fig. 1: **a** DJF, **b** MAM, **c** JJA, **d** SON. Units are percent of reference (1961–1990) values for mean and intensity of precipitation and number of days for the number of wet days

and scenarios, except in JJA, when we find a predominant increase in temperature interannual variability. This increase is particularly pronounced and mostly statistically significant in the central and eastern European regions as well as the Iberian and Balkan Peninsulas, especially for the A2 scenario. Statistically significant increases in temperature variability are also found over the Iberian Peninsula in DJF (A2 scenario), the eastern Europe region in MAM (both the A2 and B2 scenarios) and the northern and eastern Europe regions in SON (B2 scenario).

Figure 12 indicates that the variability increase is mostly driven by the boundary forcing from HadAM3H. In fact, the RegCM exhibits mostly smaller changes in interannual variability than HadAM3H, especially in summer. This indicates that the RegCM tends to reduce the variability increase signal from the large-scale HadAM3H fields. It is difficult to identify the causes for this difference, which may be related to the aforementioned stronger surface–troposphere coupling in the RegCM. We have already noted that this effect contributes to reducing the mean temperature change in the regional climate model and possibly it also contributes to reduce the change in interannual variability.

For precipitation (Fig. 13), we find a predominant increase in interannual variability (as measured by the

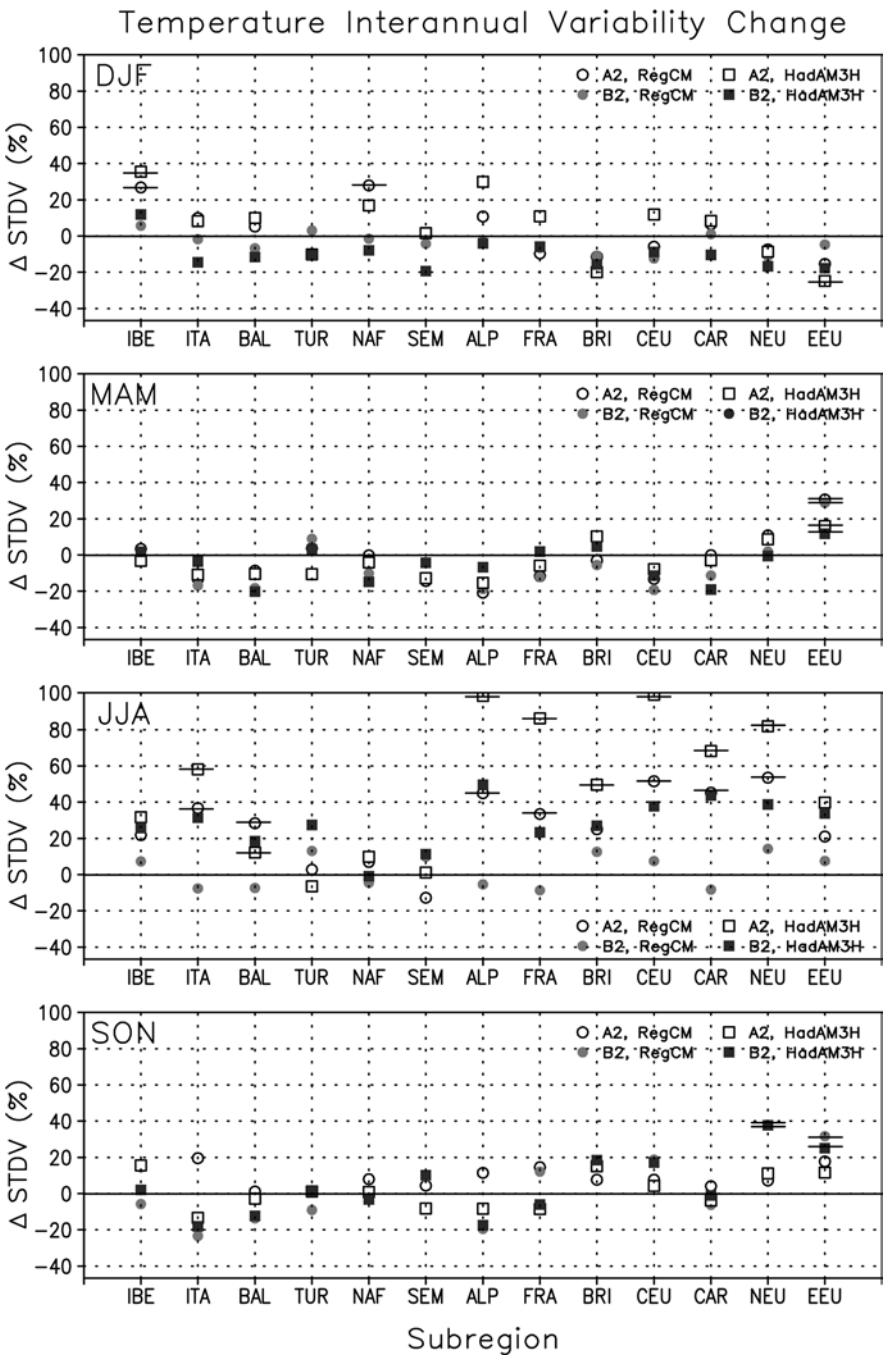

Fig. 12 Change in surface air temperature interannual standard deviation (STDV) averaged over the 13 regions of Fig. 1 for the A2 and B2 scenarios and the HadAM3H and RegCM simulations: **a** DJF, **b** MAM, **c** JJA, **d** SON. Units are °Celsius. The standard deviation is taken as a measure of the surface air temperature interannual variability. The *small horizontal bars* indicate cases in which the change is statistically significant at the 90% confidence level based on a standard *F*-test (vonStorch and Zwiers 1999)

coefficient of variation) in all seasons. The noticeable exceptions to this finding are the continental regions in DJF, where the coefficient of variation decreases while the mean precipitation and the precipitation frequency increases (see Fig. 9). These results are consistent with the theoretical expectation of a decrease (increase) in the coefficient of variation as the number of precipitation days increases (decreases) (Räisänen 2002). Consistently with temperature, also for precipitation the largest variability increase signal is found in JJA, when this increase is statistically significant at the 90% confidence level over a number of regions. Also consistent with the temperature results is the fact that the variability change signal is more pronounced in HadAM3H than in the RegCM. The surface hydrologic and energy cycles are intimately connected, and the JJA changes in both these cycles appear more intense in HadAM3H than in the RegCM over Europe.

Because of the design of the scenario experiments, changes in interannual variability cannot be attributed to changes in SST variability, since the SST interannual variations are the same in the reference and scenario simulations (see Sect. 2). Therefore these changes are dominated by corresponding changes in regional circulations or changes in the regional energy and hydrologic budgets. It is well known that the climate variability of

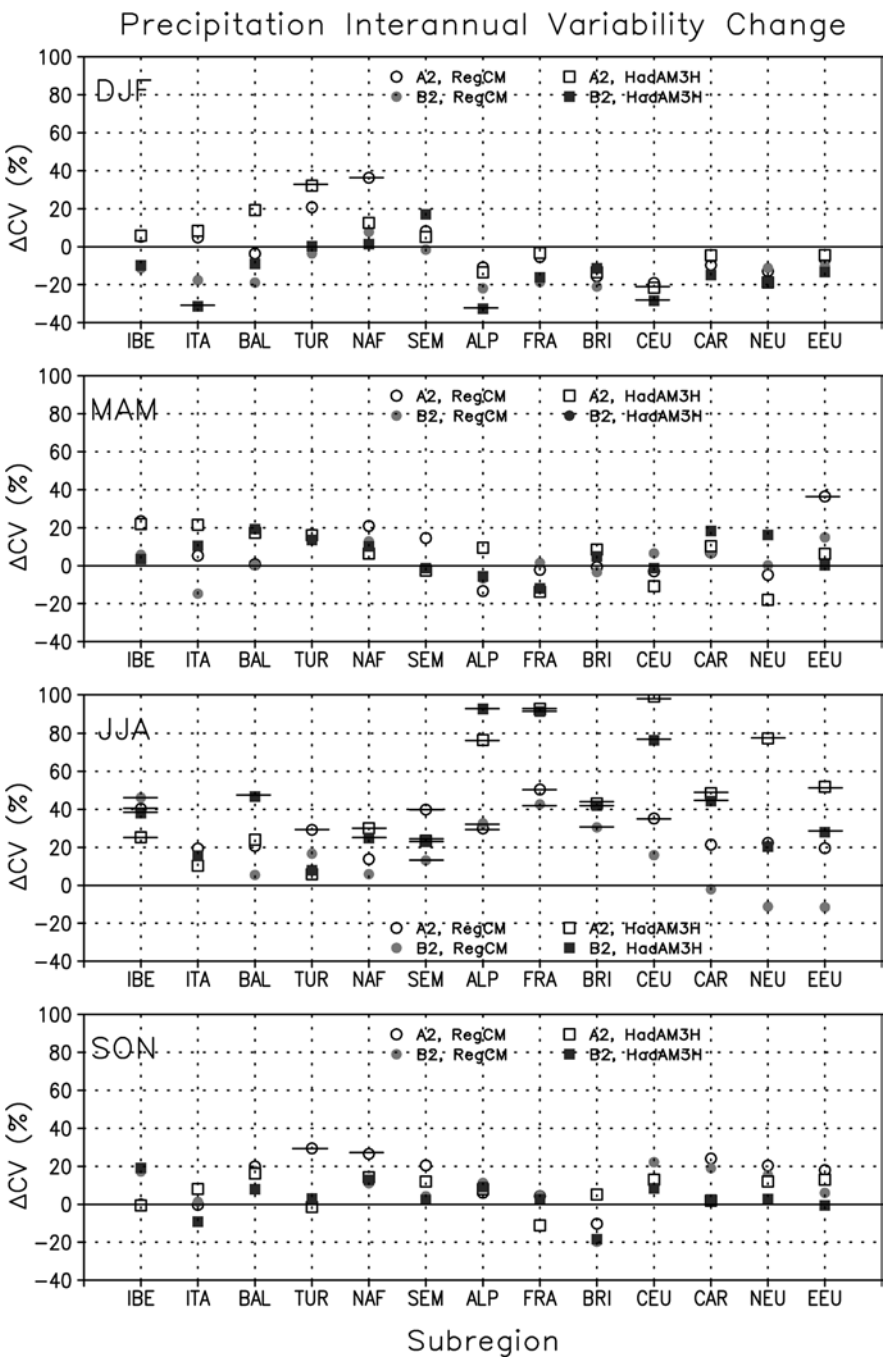

Fig. 13 Change in precipitation coefficient of variation (CV) averaged over the 13 regions of Fig. 1 for the A2 and B2 scenarios and the HadAM3H and RegCM simulations: **a** DJF, **b** MAM, **c** JJA, **d** SON. Units are percent of reference (1961–1990) values. The coefficient of variation is taken as a measure of the precipitation interannual variability. The *small horizontal bars* indicate cases in which the change is statistically significant at the 90% confidence level based on a standard *F*-test (vonStorch and Zwiers 1999)

Europe is strongly influenced by the North Atlantic Oscillation (NAO). However, this effect occurs mostly in the winter and the winter changes in variability are generally small in our simulations. This may be an indication that processes related to the NAO in the model do not undergo strong variations in the scenario runs compared to the reference run. We are currently analyzing the NAO signal in these simulations to report in a separate paper.

The fact that, in general, the variability changes in the colder seasons are relatively small might indeed be an indication that the SST forcing is an important component of this variability and our model experiment design thus prevents the occurrence of large changes. This is not the case in summer, when evidently the SST forcing is less critical and the local energy and hydrologic cycles play a more important role. We have seen in Sect. 3.1 that the summer change over Europe is characterized by a general decrease of storminess and precipitation. The increase in the coefficient of variation shown by Fig. 13, is therefore indicative of a broadening of the seasonal precipitation distribution. In other words, even in a scenario of substantially decreased average precipitation relatively wet seasons may still occur, a result consistent with a general picture of increased levels of atmospheric moisture and intensified

energy and hydrologic cycles. Feedbacks between precipitation and soil moisture, particularly in the drier conditions found in the scenario simulations, may contribute to increase the summer variability.

3.4 Trends in the scenario simulations

In this section, we present a brief analysis of the simulated trends in the 30-year scenario experiments, which can provide useful information for potential users of the data resulting from our simulations.

We limit the analysis in this section to the DJF and JJA seasons in which, as mentioned, the climate change signal is most pronounced. In addition, in order to reduce the effect of the variability associated with grid point values, we calculate the trends for temperature and precipitation averaged over the 13 regions of Fig. 1. Statistical significance at the 90% confidence level for each trend is also calculated using a two-tailed *t*-test as described by Edwards (1984).

The temperature and precipitation trends are shown in Fig. 14 for the RegCM and HadAM3H simulations. Focusing on temperature first, as expected in DJF the trends are generally of similar magnitude in the RegCM and HadAM3H simulations. Also, the trends are mostly positive and of similar magnitude in most regions for the A2 and B2 scenarios. A number of statistically significant DJF temperature trends of about 0.5°C/decade are found in both scenario simulations.

A different picture is seen in the JJA temperature trends. In JJA, we find greater differences between the A2 and B2 scenarios and between the HadAMH and RegCM simulations. In the B2 scenario the JJA temperature trends are generally small (less than 0.5°C/decade) in both models and they are not statistically significant. However, in the A2 scenario the regional trends are large, between 0.5 and 1.5°C/decade, they are all statistically significant at the 90% confidence level and they are generally larger in the HadAM3H than in the RegCM. This result is consistent with the greater JJA temperature mean and variability changes found in HadAM3H than in the RegCM (see Figs. 8 and 12).

Moving our attention to the precipitation trends of Fig. 14, we find that only in a few cases the regional precipitation trends are statistically significant at the 90% confidence level throughout the scenario simulations. These include the positive DJF precipitation trends over the Iberian Peninsula, Italian Peninsula and France region in the B2 scenario and the JJA drying trend over the Alpine, northern Africa and central European regions in the A2 scenario. Mostly, the RegCM and HadAM3H trends are in agreement with each other, as these trends are essentially determined by corresponding trends in large scale circulations and water vapor loadings.

A message from Fig. 14 is that the interdecadal characteristics of the B2 and A2 simulations can be quite different from each other at the regional scale. This can be due to either the different magnitude and nature of forcings in the two scenarios or to the natural interdecadal variability of the climate system. Ensemble simulations would be needed to examine this issue.

4 Summary and conclusions

In this paper, we analyzed the climatic changes simulated over the European region under two IPCC emission scenarios (A2 and B2) for the period 2071–2100 with respect to the reference period 1961–1990. The simulations are performed with the regional climate model RegCM using forcing lateral boundary conditions from time-slice simulations with the HadAM3H global atmospheric model. Our primary conclusions can be summarized as follows:

1. In all seasons, Europe undergoes warming in both the A2 and B2 scenarios. The warming is in the range of 2.5–5.5°C in the A2 scenario and 1–4°C in the B2 scenario. The warming is maximum over eastern Europe in DJF and over western and southern Europe in JJA. The seasonal warming values in the two scenarios scale by a factor varying mostly from 1.3 to 1.7 over different subregions.
2. The precipitation changes vary substantially from season to season and across regions in response to changes in large scale circulations and water vapor loadings. In DJF, increased Atlantic cyclonic activity leads to enhanced precipitation over much of western, central and northern Europe (up to 15–30%). DJF precipitation is reduced over the southern Mediterranean regions in response to increased anticyclonic circulation there. In JJA, an enhanced anticyclonic circulation is found over the northeastern Atlantic which induces a ridge over western Europe and a trough over eastern Europe. This blocking-like structure deflects storms northward, causing a substantial and widespread decrease of precipitation over western and central Europe as well as the Mediterranean Basin (up to 30–45%). Both the DJF and JJA changes are statistically significant at the 95% confidence level over extended areas of our domain. Relatively small precipitation changes are found in the intermediate seasons of MAM and SON (within $\pm 15\%$). The precipitation changes we find in our simulation appear qualitatively consistent with a number of previous climate change experiments.
3. Except for DJF over the western, central and eastern European regions (when both the precipitation intensity and frequency increase) we find a predominant increase in the intensity of daily precipitation events and a decrease in the frequency of events, also in areas where the mean precipitation decreases. This implies not only shifts but also changes in the shape of the intensity distribution of precipitation events.
4. In general, the interannual variability increases in the scenario simulations during the summer, while it

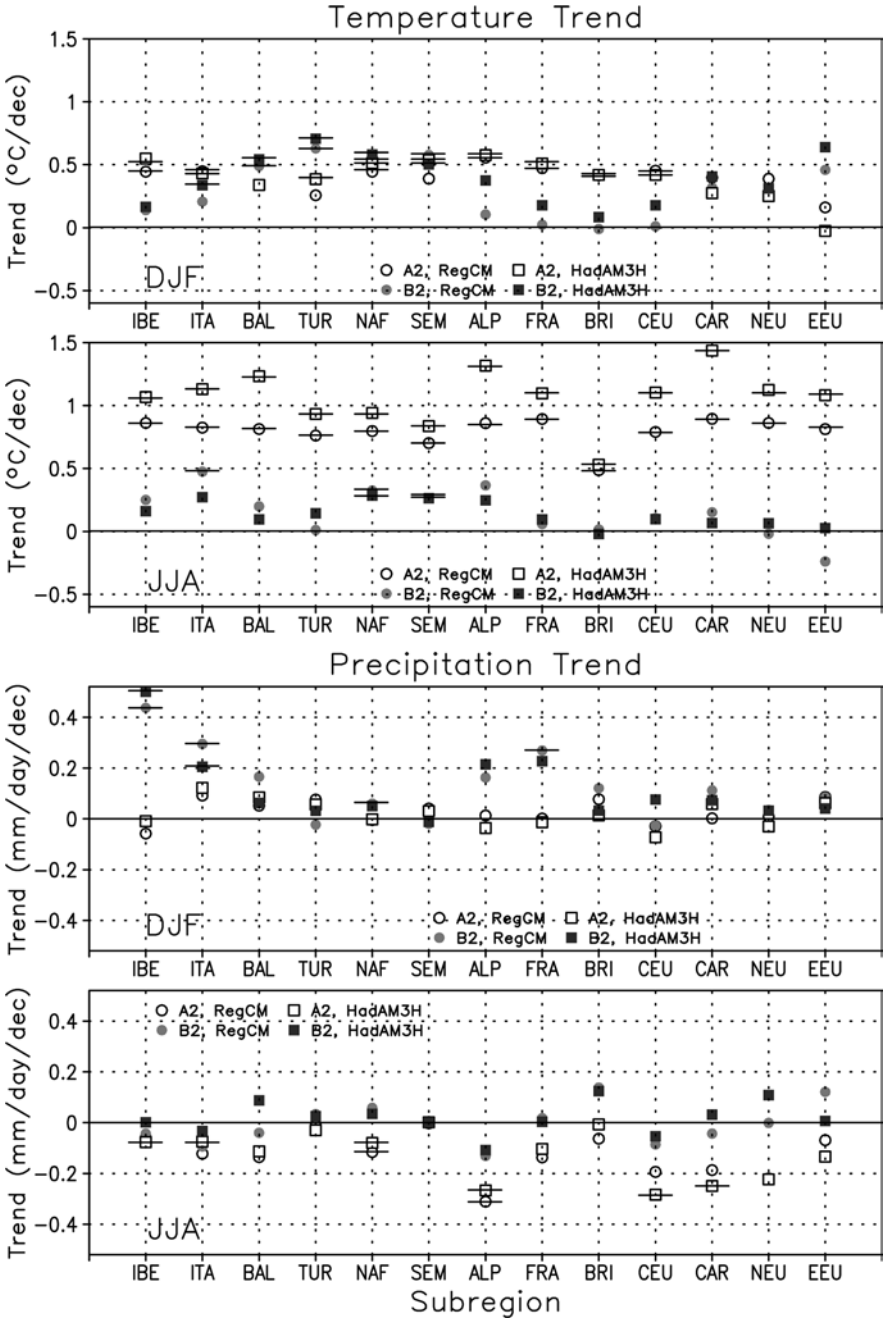

Fig. 14 Linear trend values throughout the A2 and B2 RegCM and HadAM3H simulations for surface air temperature °C/decade) and precipitation (mm/day/decade) averaged over the 13 regions of Fig. 1: **a** temperature trend, DJF, **b** temperature trend, JJA, **c** precipitation trend, DJF, **d** precipitation trend, JJA. The *small horizontal bars* indicate cases in which the trend is statistically significant at the 90% confidence level based on a two-tailed *t*-test (Edwards 1984)

shows only small changes in the other seasons. Because of our experiment design, this increase is not attributable to changes in interannual variability of SSTs.

5. A number of statistically significant trends were found within the scenario simulations over different sub-regions of our domain, most noticeably for temperature in both DJF (both scenarios) and JJA (A2 scenario).
6. Cloudiness, snow cover and soil-water content tend to predominantly decrease in the scenario simulations, often also in areas where precipitation increases. This result is in agreement with the continental interior drying found in a number of global climate change simulations (Cubasch et al. 2001).
7. The broad patterns of change in the nested RegCM and driving HadAM3H fields are generally consistent with each other, as can be expected from the strong influence of the boundary forcing on the regional model simulation. In JJA, however, when local physical processes are most important, significant differences in the temperature and precipitation change can be found between the models. In particular, the RegCM simulates smaller changes in both the mean and interannual variability of surface climate. The climate change signal in the RegCM simulation exhibits substantial fine scale

detail induced by local topographical and coastline forcing, both for precipitation and surface air temperature. In addition, sharp gradients in the change signals are found, especially for precipitation (e.g. in DJF). This indicates that high-resolution detail is necessary for an accurate simulation of climate change over Europe. Such detail is typically better simulated by high resolution RCMs than coarse resolution global models (e.g. Giorgi and Marinucci 1996; Jones et al. 1997; Giorgi and Mearns 1999).

Our simulations included the direct and indirect effects of sulfate aerosols. It is difficult to evaluate the influence of these aerosol effects on the change signals, since this would require a comparison with aerosol-free simulations. The regional model studies of Giorgi et al. (2002, 2003a) and Ekman and Rodhe (2003) indicate that sulfate aerosols can produce regional surface coolings ranging from several tenths of a degree to more than 1°C. In the change signals, however, the aerosol effects partially cancel out, especially because the concentration of aerosols in the A2 and B2 scenarios, after reaching a maximum in the first several decades of the twenty-first century, tends to decrease in the latter decades to levels close to, or even lower than, the present day values (IPCC 2000). Therefore, we speculate that the sulfate aerosol effects have a secondary contribution to the changes found in the present experiments.

Our results indicate that both in the A2 and B2 scenarios the climate of Europe might undergo substantial changes which can have profound impacts on human activities and natural systems. In particular some of the changes we find, most noticeably the maximum summer warming and drying over the western European and Mediterranean regions, the increase of winter precipitation over western, central and northern Europe and the predominant increase in the intensity of precipitation events, are consistent with a number of previous simulations. This suggests a robustness in these regional signals, which will be better assessed when our simulations are compared with the full set of global and regional model simulations participating to the PRUDENCE project.

Acknowledgements This work was supported by the European Union Programme Energy, Environment and Sustainable Development under contract EVK2-2001-00156 (PRUDENCE). We would like to thank the Hadley Centre for providing the HadAM3H data. We also thank two reviewers for their insightful comments which helped to improve the quality of the paper.

References

Beniston M (2004) The 2003 heat wave in Europe: a shape of things to come? An analysis based on Swiss climatological data and model simulations. Geophy Res Lett 31(2):L02202. DOI 10.1029/2003GL018857

Christensen JH, Christensen OB (2003) Climate modelling: severe summertime flooding in Europe. Nature 421:805–806

Christensen JH, Carter TR, Giorgi F (2002) PRUDENCE employs new methods to assess European climate change. EOS 83:147

Cubasch U, Meehl GA, Boer GJ, Stouffer RJ, Dix M, Noda A, Senior CA, Raper S, Yap KS (2001) Projections of future climate change. In: Houghton JT, Ding Y, Griggs DJ, Noguer M, van der Linden PJ, Dai X, Maskell K, Johnson CA (eds). Climate change 2001; the scientific basis, contribution of working group I to the third assessment report of the intergovernmental panel on climate change (IPCC) chapt. 9. Cambridge University Press, Cambridge, pp 525–582

Edwards AL (1984) An introduction to linear regression and correlation. WH Freeman and Co., New York, pp 81–83

Ekman AML, Rodhe H (2003) Regional temperature response due to indirect sulfate aerosol forcing: impact of model resolution. Clim Dynam 21:1–10

Giorgi F, Marinucci MR (1996) Improvements in the simulation of surface climatology over the European region with a nested modeling system. Geophys Res Let 23:273–276

Giorgi F, Mearns LO (1999) Introduction to special section: regional climate modeling revisited. J Geophys Res 104:6335–6352

Giorgi F, Mearns LO (2002) Calculation of average, uncertainty range and reliability of regional climate changes from AOGCM simulations via the "Reliability Ensemble Averaging (REA)" method. J Clim 15:1141–1158

Giorgi F, Marinucci MR, Visconti G (1992) A 2XCO2 climate change scenario over Europe generated using a limited area model nested in a general circulation model II: climate change scenario. J Geophys Res 97:10011–10028

Giorgi F, Marinucci MR, Bates GT (1993a) Development of a second generation regional climate model (RegCM2). Part I: boundary-layer and radiative transfer processes. Mon Wea Rev 121:2794–2813

Giorgi F, Marinucci MR, Bates GT, De Canio G (1993b) Development of a second generation regional climate model (RegCM2). Part II: convective processes and assimilation of lateral boundary conditions. Mon Wea Rev 121:2814–2832

Giorgi F, Hurrell JW, Marinucci MR, Beniston M (1997) Elevation signal in surface climate change: a model study. J Clim 10:288–296

Giorgi F, Whetton PW, Jones RG, Christensen JH, Mearns LO, Hewitson B, vonStorch H, Francisco R, Jack C (2001) Emerging patterns of simulated regional climatic changes for the 21st century due to anthropogenic forcings. Geophys Res Lett 28: 3317–3320

Giorgi F, Bi X, Qian Y (2002) Direct radiative forcing and regional climatic effects of anthropogenic aerosols over East Asia: a regional coupled climate-chemistry/aerosol model study. J Geophys Res 107:4439. DOI 10.1029/2001JD001066

Giorgi F, Bi X, Qian Y (2003a) Indirect vs. direct effects of anthropogenic sulfate on the climate of East Asia as simulated with a regional coupled climate-chemistry/aerosol model. Climatic Change 58:345–376

Giorgi F, Bi X, Pal JS (2004) Mean, interannual variability and trends in a regional climate change experiment over Europe. I: present day climate (1961–1990). Clim Dyn 22:733–756

Huntingford C, Jones RG, Prudhomme C, Lamb R, Gash JHC, Jones DA (2003) Regional climate model predictions of extreme rainfall for a changing climate. Q J R Meteorol Soc 129:1607–1622

IPCC (2000) Emission scenarios, a special report of working group III of the intergovernmental panel on climate change. Nakicenovic N, Coordinating Lead Author, Cambridge University Press, Cambridge, p 599

Johns TC, Gregory JM, Ingram WJ, Johnson CE, Jones A, Mitchell JFB, Roberts DL, Sexton DMH, Stevenson DS, Tett SFB, Woodage MJ (2001) Anthropogenic climate change for 1860 to 2100 simulated with the HadCM3 model under updated emission scenarios. Hadley Centre Technical Note no. 22, p 62

Jones RG, Murphy JM, Hassell D, Taylor R (2001) Ensemble mean changes in a simulation of the European mean climate of 2071–2100 using the new Hadley Centre regional modeling system HadAM3H/HadRM3H. Hadley Centre report, p 19

Jones RG, Murphy JM, Noguer M, Keen M (1997) Simulation of climate change over Europe using a nested regional climate model. I: comparison of driving and regional model responses to a doubling of carbon dioxide. Q J R Meteorol Soc 123:265–292

Leung LR, Ghan SJ (1999) Pacific Northwest climate sensitivity simulated by a regional climate model driven by a GCM. Part II: 2XCO2 simulations. J Clim 12:2031–2053

Loveland TR, Merchant JW, Ohlen DO, Brown JF (1991) Development of a land cover characteristics database for the conterminous United States. Photogrammetric Eng Remote Sensing 57:1453–1463

Mitchell JFB, Johns TC, Eagles M, Ingram WJ, Davis RA (1999) Towards the construction of climate change scenarios. Clim Change 41:547–581

Pal JS, Small EE, Eltahir EAB (2000) Simulation of regional—scale water and energy budgets: representation of subgrid cloud and precipitation processes within RegCM. J Geophys Res 105:29579–29594

Pope VD, Gallani ML, Rowntree PR, Stratton RA (2000) The impact of new physical parameterisations in the Hadley Centre climate model. Clim Dynam 16:123–146

Räisänen J, Joelsson R (2001) Changes of average and extreme precipitation in two regional climate model experiments. Tellus A 53:547–566

Räisänen J, Rummukainen M, Ullerstig A (2001) Downscaling of greenhouse gas induced climate change in two GCMs with the Rossby Centre regional climate model for northern Europe. Tellus A 53:168–191

Räisänen J (2002) CO_2-induced changes in interannual temperature and precipitation variability in 19 CMIP2 experiments. J Clim 15:2395–2411

Räisänen J, Hansson U, Ullerstig A, Döscher R, Graham LP, Jones C, Meier HEM, Samuelsson P, Willen U (2004) European climate in the late twenty-first century: regional simulations with two driving global models and two forcing scenarios. Clim Dynam 22:13–31

Schär C, Vidale PL, Luthi D, Frei C, Haberli C, Liniger MA, Appenzeller C (2004) The role of increasing temperature variability in European summer heatwaves. Nature 427:332–336

vonStorch H, Zwiers FW (1999) Statistical analysis in climate research. Cambridge University Press, Cambridge, p 484